1st Pan-American Congress on Computational Mechanics - PANACM 2015
XI Argentine Congress on Computational Mechanics - MECOM 2015
S. Idelsohn, V. Sonzogni, A. Coutinho, M. Cruchaga, A. Lew & M. Cerrolaza (Eds)

ATOMISTIC STUDY OF THE MECHANICAL PROPERTIES OF A SINTERED BULK METALLIC GLASS (NANOGLASS)

FRANCO ARDIANI[1], ANDRÉS A. MANELLI[1], CARLOS J. RUESTES[2], CLAUDIO A. CAREGLIO[1,3] AND EDUARDO M. BRINGA[2,4]

[1]Facultad de Ingeniería, Universidad Nacional de Cuyo
Centro Universitario, 5500 Mendoza, Argentina
francoamg@gmail.com, andresmanelli@gmail.com, ccareglio@uncu.edu.ar

[2]ITIC, Universidad Nacional de Cuyo
Centro Universitario, 5500 Mendoza, Argentina

[3]FCEN, Universidad Nacional de Cuyo
Centro Universitario, 5500 Mendoza, Argentina
cjruestes@hotmail.com, diego.tramontina@gmail.com, ebringa@yahoo.com

[4]CONICET
5500 Mendoza, Argentina

Key words: Metallic Glasses, Large Deformations, Porosity, Atomistic Analysis

Abstract. Metallic glasses with porosity have been in the spotlight in recent years and much research has been done on them, in an effort to improve the understanding of the mechanics of deformation. The behavior of the material in the elastoplastic regime may be controlled by the introduction of pores, thus the interest on simulating them.

Large deformation is normally a consequence of shear transformations zones (STZ) collapsing into shear bands (SB) which may lead to catastrophic failure. It is widely known that in crystalline metals the addition of nanopores slows down dislocation motion and changes the resulting plastic deformation. Similarly, pores in metallic glasses limit the propagation of shear bands and allow a more homogeneous deformation.

In previous work we determined constitutive parameters of the Cu_{46} Zr_{54} metallic glass as a function of temperature. We now present results for a metallic glass with the same composition, but fabricated by sintering of BMG nanoparticles, which results in samples with porosity, similar to nanoglass samples in some experiments and simulations. Atomistic simulations are carried out using Molecular Dynamics (MD), and analysis includes atomic Voronoi polyhedra, and atomic stress and strain. We analyse the dependence of deformation on solid volume fraction, and the way deformation is distributed throughout the sample, as a function of initial porosity.

1 INTRODUCTION

A Metallic Glass (MG), also called "amorphous metal", is a metallic alloy which exhibits an amorphous structure, contrary to the most usual crystalline structure of metals. This may be accomplished by several techniques, most of which include high quenching rates, low volumes and composition control [1]. As a result, these materials have some advantages over crystalline metals, such as improved elasticity combined with high resistance, strength and moldability [2].

There are two main approaches to computationally simulate MGs under plastic strain: focusing on nanoscale behavior [3, 4] or using continuum mechanics [5]. For the first approach, Molecular Dynamics (MD) simulations are often used [6]. MD solves problems with many bodies by applying an atom to atom potential, thus being useful to study nanoscale properties, such as strain, stress, temperature, etc.

MD simulations are also useful to identify plastic processes in BMGs (Bulk Metallic Glasses). Plasticity in BMGs starts with the formation of Shear Transformation Zones (STZ), which nucleate into shear bands [3, 7] with increasing strain. Shear bands (SB) may lead to brittle failure of the material due to heterogeneous deformation, thus the importance of preventing their propagation. In crystalline metals a similar thing is done with dislocations.

A more homogeneous deformation may be achieved by adding nanoinclusions to the material. There has been great interest in this subject lately, and many options have been explored [8, 9, 10, 11]. Following previous work [12], we now fabricate Cu_{46} Zr_{54} BMG samples with porosity (similar to nanoglass samples in other experiments and simulations [13, 14]) by sintering of nanoparticles. MD simulations will allow us to analyse atomic Voronoi polyhedra, atomic stress and strain, and the way initial porosity affects the deformation of the sample.

2 SIMULATION DETAILS AND POROUS SAMPLE PREPARATION

For this paper, MD simulations were carried out using the LAMMPS software [15], which is free and open source, has an excellent manual, and is computationally efficient in the simulation of systems with large numbers of atoms. In addition Voronoi analysis and images of the sample were made with Ovito software [16], and other figures were plotted with Gnuplot, both of these softwares also being free and open source.

For the preparation of the porous sample, we started from the sample used in previous work [12] and described by Arman [17]. It is a Cu_{46} Zr_{54} prismatic sample with a total of about 160000 atoms and obtained with a cooling rate of 10^{12} K/s. The experimental glass transition temperature (T_g) of this metallic glass is 696 K, and the experimental shear modulus (G) is 30 GPa [18]. To describe the interactions between atoms, an embedded atom method (EAM) potential [19] is adopted. We use 3D periodic boundary conditions, suitable for high strain rates [20], so as to simulate a BMG and avoid stress concentration at the boundaries.

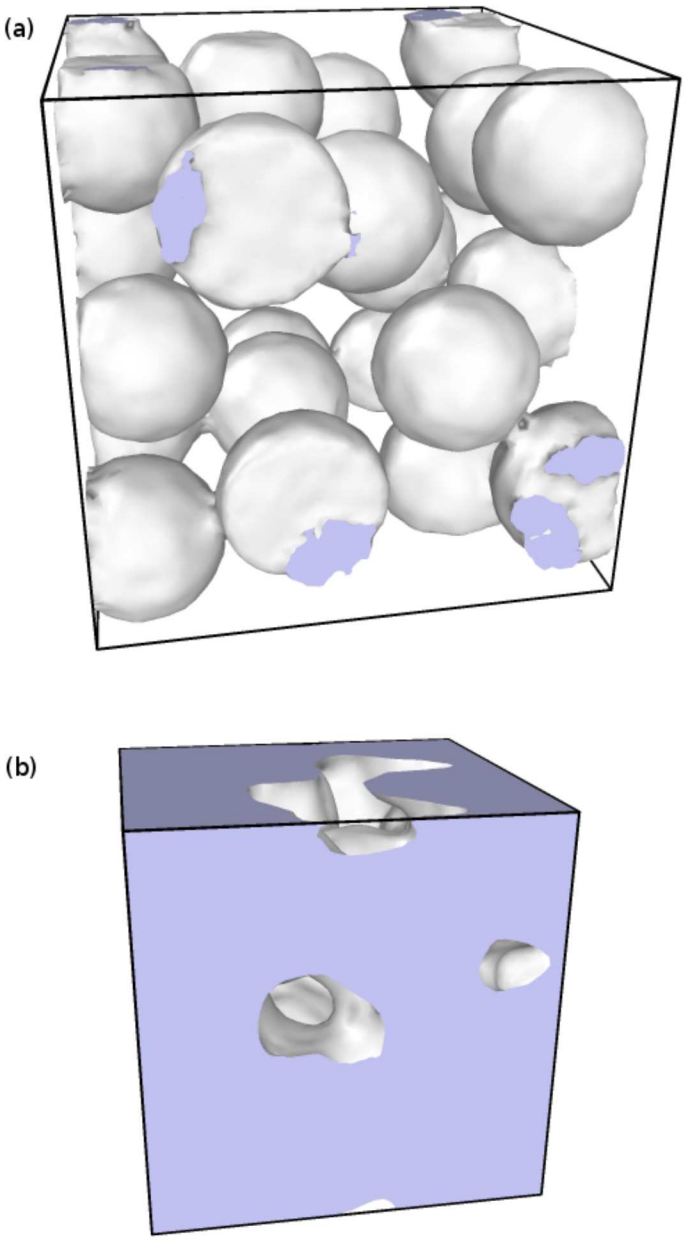

Figure 1: Images of the sample (a) prior to sintering process and (b) after sintering process (13% porosity).

We took the original sample and replicated it along one direction so as to obtain a roughly cubic sample, with a side of about 15 nm. Afterwards, we randomly selected points within this sample which would be the center of spheres (2.5 nm radius), and remove all atoms outside those spheres in order to simulate sintering of spherical glass

nanoparticles. Figure 1-(a) shows the sample prior to the sintering process. This sample has 77888 atoms.

The procedure for the simulated sintering was to relax the sample at a constant high-temperature of 650K, just below the glass temperature, at constant volume during few ps, and then apply up to 10 ps of compressive pressure (400 bar). We then repeated these two steps until the desired porosities were obtained. Then, we performed further relaxation with the following procedure: cooling from the sintering temperature to zero temperature at a rate of $6.5 \cdot 10^{14} K/s$, applying a barostat to reach zero pressure, heating at the same rate than the cooling rate to arrive to the desired simulation temperature (300K) and, finally, applying a barostat during 5 ps to reduce pressure to zero while maintaining constant temperature. Figure 1-(b) shows one of the samples that result from the mentioned sintering procedure.

Samples with different initial porosities (3.3%, 5.8% and 13.1%) were prepared. These stable samples were then used to perform uniaxial compressive and tensional loading. All atomic coordinates were scaled every step, according to the desired strain rate, which in this case was $10^9/s$, appropiate for shock compression experiments.

3 RESULTS

Below we present results for purely uniaxial strain, which is adequate for the comparison with results of experiments at very high strain rates, where lateral strains can be neglected during loading.

Figure 2-(a) plots Pressure along the Z-axis (loading axis) versus strain for compressive strain. The presence of porosity helps the initiation of plasticity, due to pores acting as shear concentrators, thus facilitating the appearance of STZs and shear bands. This early plasticity starts to close out the pores, producing a curve where the strain increases while maintaining low pressure. When the pores close, the pressure increases in a more accelerated manner, as shown by the portion of curve after the dashed lines. Moreover, we can as well observe that the behavior of the porous curves after the dashed lines matches the behavior of the non-porous curve, implying there is no more porosity. Based on the figure, we can conclude that, with increasing porosity, less pressure is needed to close the pores (height of the dashed lines), but this happens at a higher strain.

Under tensile strain, the sample behaves quite differently. We have found, from the analysis of snapshots of the sample (as those seen in Figure 5), that pores do not close under tension as they did under compression. What is more, they seem to grow at a roughly constant rate with increasing strain. The use of periodic boundary conditions precludes the closing of the voids even at 20% uniaxial strain, given that there is no lateral strain. Figure 2-(b) shows what seems to be plastic flow: particularly for 13% porosity, but seemingly for the other porosities, after a certain point, strain increases while pressure stays constant or even decreases.

Figure 3 shows Voronoi polyhedra-strain curves. The Voronoi tesselation analysis is a technique for characterizing short range order in amorphous metallic glasses, where each

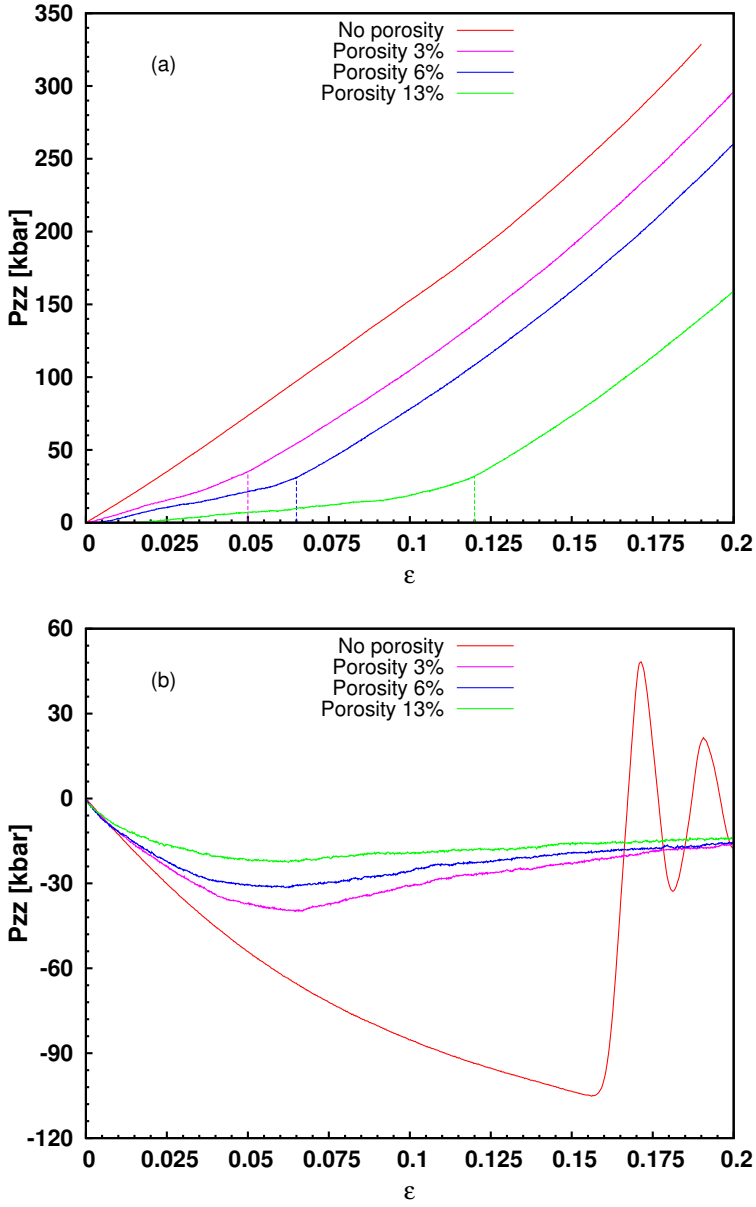

Figure 2: Pressure on Z axis-strain curves. (a) Compression (b) Tension.

atom is the center of a Voronoi polyhedron, formed of its nearest neighbors. In [17], type 3 atoms are identified as plasticity indicators, thus their importance.

Figure 3-(a) shows Voronoi polyhedra for compressive strain. This figure shows a fall in the number of Type 3 atoms after a constant stage. This has been thought to be an indicator of the onset of plasticity [17]. However, our graphic shows a counter-intuitive result, as plasticity starts earlier in the samples with less porosity according to this Voronoi

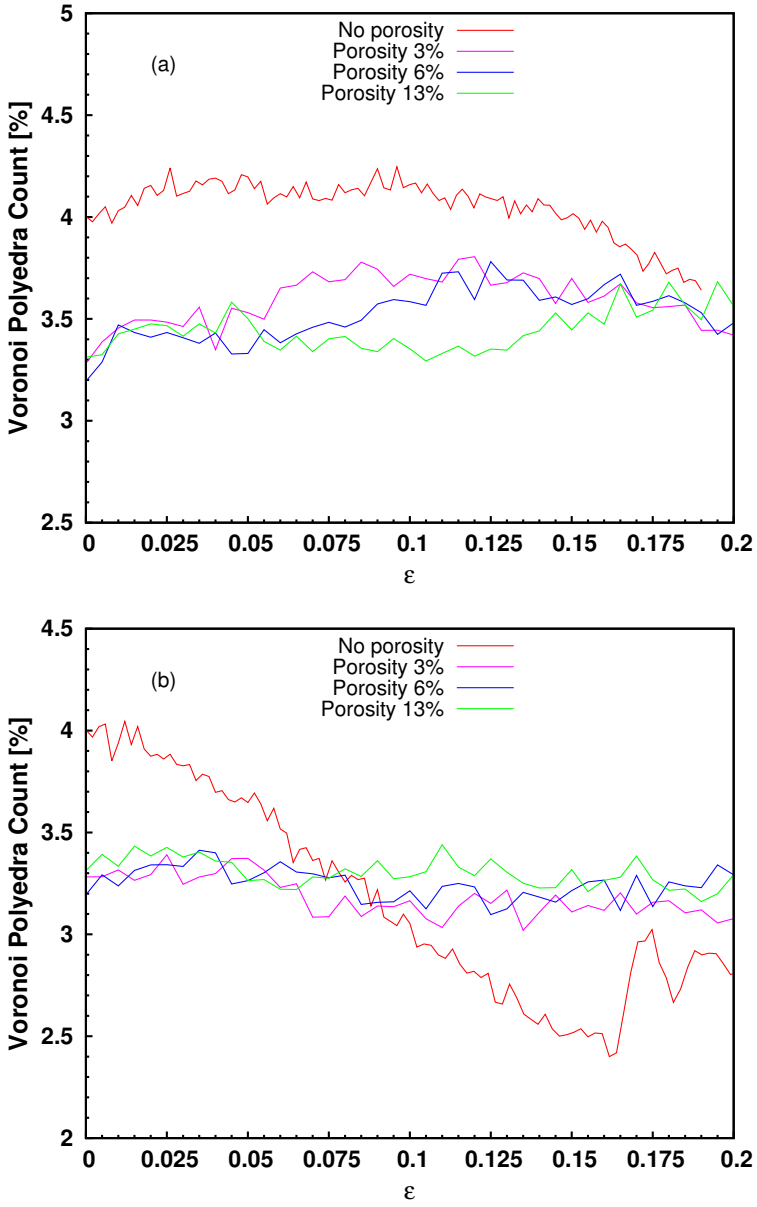

Figure 3: Type 3 Voronoi polyhedra-strain curves. (a) Compression (b) Tension.

analysis. This could be considered as an indicator that there are other processes involved in early stages of deformation that have an influence in the results.

Figures 4-(b) and (c) show the evolution of shear strain in the sample, for compressive strain. We can easily observe that pores act as stress concentrators, but they also represent an obstacle for shear band propagation [9]. Shear bands form diagonally from pore to pore, and the atomic strain continues to accumulate along this directions for the rest of

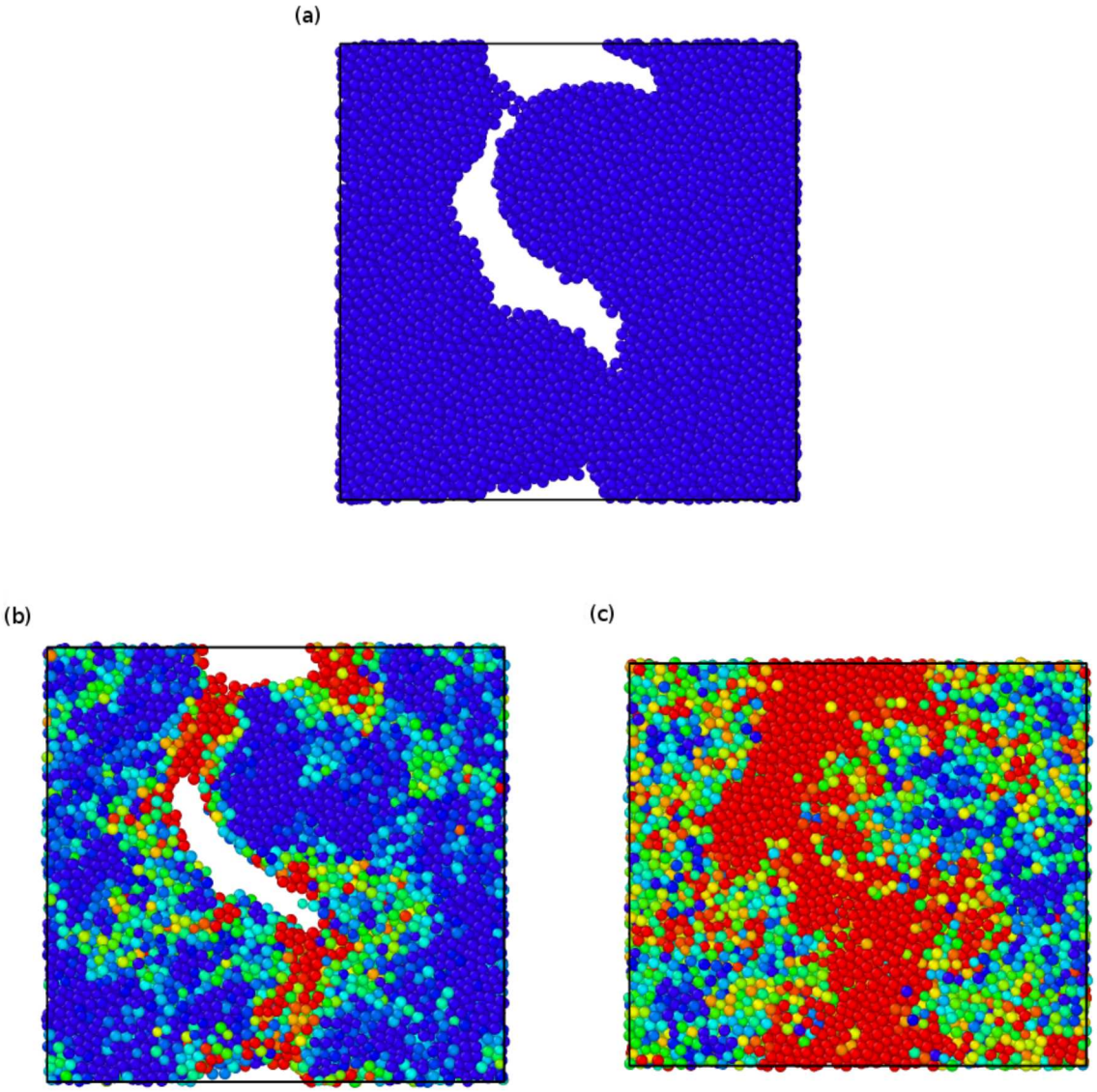

Figure 4: Shear strain coloring of the 13% porosity sample's slice. The shear strain coloring was made using ovito, blue is 0.1 or less and red is 0.3 or more shear strain. (a) 0% strain (b) 5% compressive strain (c) 12% compressive strain.

the loading, as shown by the bulk glass at 12% strain. Hardening appears moments before the total closure of the pores as has been pointed out by [21] and can be appreciated in Figure 2-(a).

Figure 3-(b) shows Voronoi polyhedra for tensile strain. In this figure, type 3 atoms show practically no variation for the porous samples, which would imply that no STZs are

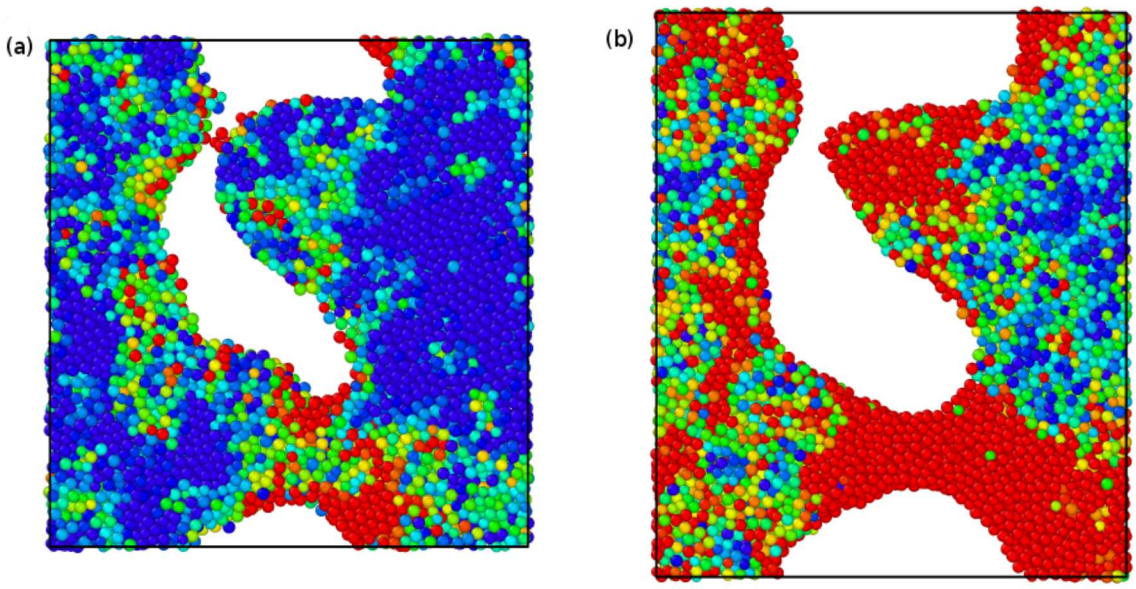

Figure 5: Shear strain coloring of the 13% porosity sample's slice. The shear strain coloring was made using ovito, blue is 0.1 or less and red is 0.3 or more shear strain. (a) 6% tensile strain (b) 20% tensile strain.

being formed. For the non-porous sample, the count of type 3 atoms becomes somewhat constant after the void has been nucleated. This led us to think that, given the conditions for the samples, the movement of the atoms around the pores is facilitated, and prevents the formation of STZs other than the ones around the pores. To support this idea, in Figures 5-(b) and (c) we show the sample colored for shear strain. It is evident that shear strain is mostly concentrated around the pores. It should be mentioned that the relative position between atoms far from the pores remains almost the same.

4 CONCLUSIONS

Molecular Dynamics (MD) simulations were carried out on a porous Cu_{46} Zr_{54} metallic glass sample, applying compressive and tensile loading. The results under strain were comparable to those found in the literature [21] for compresion of porous monocrystalline Cu samples. This could be considered as validation of the sintering process used to prepare the nanoglass samples.

Under compression, pores facilitate the plastic process acting as stress concentrators, but they delay as well the formation of Shear Transformation Zones (STZs) and their possible union into a full shear band (SB), for the material far from the pores. Results also show hardening of the sample following the total closure of the pores, very much similar to the non-porous case.

Under tension, and using purely uniaxial strain, pores do not close and they concentrate plastic flow around them, also impeding the formation of STZ and SBs.

Future study will also include a deeper Voronoi analysis and simulations of larger samples, with different void topologies.

5 ACKNOWLEDGEMENTS

We all thank support from SeCTyP-UNCuyo grant "B008 Study of possible improvements of the mechanical properties of metallic glasses". EMB and CJR also thank support from PICT-PRH 0092.

REFERENCES

[1] Liebermann H., *Rapidly Solidified Alloys*. Marcel Dekker, Inc, New York (1993).

[2] Telford M., The case for bulk metallic glass. *Materials Today*, **7(3)**:36-43 (2004).

[3] Ogata S. et al., Atomistic simulation of shear localization in CuZr bulk metallic glass. *Intermetallics*, **14**:1033-1037 (2006).

[4] Guan P., Stress-Temperature Scaling for Steady-State Flow in Metallic Glasses. *Phys. Rev. Lett.*, **104**, 205701 (2010).

[5] Malvern L., *Introduction to the mechanics of a continuous medium*. Prentice-Hall (1969).

[6] Allen M.P. and Tildesley D.J., *Computer simulation of liquids*. Oxford University Press (1987).

[7] Shimizu F., Ogata S. and Li J., Theory of shear banding in metallic glasses and molecular dynamics calculations. *Materials Transactions*, **48(11)**:2923-2927 (2007)

[8] P. P. Guan, S. Lu, M. Spector, P. Valavala and M. Falk, Cavitation in amorphous solids. *Phys. Rev. Lett*, **110**, 185502 (2013).

[9] J. Wang, P. Hodgson, J. Zhang, W. Yan and C. Yang, Effects of pores on shear bands in metallic glasses: A molecular dynamics study. *Comput. Mater. Sci.*, **50**:211-217 (2010).

[10] A.C. Lund and C.A. Schuh, Critical length scales for the deformation of amorphous metals containing nanocrystals. *Philosophical Magazine Letters*, **87:8**, 603-611 (2007).

[11] R. Liontas, X.W. Gu, E. Fu, Y. Wang, N. Li, N. Mara and J.R. Greer, Effects of Helium Implantation on the Tensile Properties and Microstructure of Ni_{73} P_{27} Metallic Glass Nanostructures. *Nano Lett.*, **14**:5176-5183 (2014).

[12] F. Ardiani, A. Manelli, C. Ruestes, C. Careglio and E. Bringa, Atomistic simulations of amorphous metals in the elasto-plastic regime. *Mec. Comput.*, **31**:1437-1449 (2012).

[13] S. Adibi, Z.-D. Sha, P. Branicio, S. Joshi, Z.-S. Liu and Y.-W. Zhang, A transition from localized shear banding to homogeneous superplastic flow in nanoglass. *Appl. Phys. Lett.*, **103**, 211905 (2013).

[14] K. Albe, Y. Ritter and D. Sopu, Enhancing the plasticity of metallic glasses: Shear band formation, nanocomposites and nanoglasses investigated by molecular dynamics simulations. *Mech. Mater.*, **67**:94-103 (2013).

[15] S. Plimpton, Fast parallel algorithms for short-range molecular dynamics. *J. Comp. Phys.*, **117**:1-19 (1995). Site: http://lammps.sandia.gov.

[16] A. Stukowski, Visualization and analysis of atomistic simulation data with OVITO - the Open Visualization Tool. *Modelling Simul. Mater. Sci. Eng.*, **18**, 015012 (2010). Site: http://ovito.org/.

[17] Arman B., Luo S.-N., Germann T.C. and Cain T., Dynamic response of Cu_{46} Zr_{54} metallic glass to high-strain-rate shock loading: Plasticity, spall, and atomic-level structures. *Phys. Rev. B.*, **81**, 144201 (2010).

[18] Johnson W.L., Samwer K., A universal criterion for plastic yielding of metallic glasses with a $(T/T_g)^{2/3}$ temperature dependence. *Phys. Rev. Lett.*, **95**, 195501 (2005).

[19] Daw M. and Baskes M.I., Embedded-atom method: Derivation and application to impurities, surfaces, and other defects in metals. *Phys. Rev. B.*, **29**:6443-6453 (1984).

[20] Bringa E.M. et al., Ultrahigh strength in nanocrystalline materials under shock loading. *Science*, **309**:1838-1841 (2005).

[21] F. Yuan and X. Wu, Scaling laws and deformation mechanisms of nanoporous copper under adiabatic uniaxial strain compression. *AIP ADVANCES*, **4**, 127109 (2014).

1st Pan-American Congress on Computational Mechanics - PANACM 2015
XI Argentine Congress on Computational Mechanics - MECOM 2015
S. Idelsohn, V. Sonzogni, A. Coutinho, M. Cruchaga, A. Lew & M. Cerrolaza (Eds)

MECHANICAL PROPERTIES OF A $CU_{46}ZR_{54}$ BULK METALLIC GLASS WITH EMBEDDED CRYSTALLINE NANO PARTICLES

ANDRES A. MANELLI*[1], FRANCO ARDIANI[1], CLAUDIO A. CAREGLIO[1,2] AND EDUARDO M. BRINGA[3,4]

[1]Facultad de Ingeniería, Universidad Nacional de Cuyo
Centro Universitario, 5500 Mendoza, Argentina
andresmanelli@gmail.com, francoamg@gmail.com, ccareglio@uncu.edu.ar

[2]ITIC, Universidad Nacional de Cuyo Centro Universitario, 5500 Mendoza, Argentina

[3]FCEN, Universidad Nacional de Cuyo
Centro Universitario, 5500 Mendoza, Argentina
cjruestes@hotmail.com, diego.tramontina@gmail.com,ebringa@yahoo.com

[4]CONICET
5500 Mendoza, Argentina

Key words: Computational Mechanics, Metallic Glass, Inclusions, Diffusivity

Abstract. Plasticity in bulk metallic glasses (BMGs), is normally dominated initially by shear transformations zones (STZ), which expand to form shear bands (SB) through the material. In order to control and thus improve the dynamics of plasticity, composition of metallic glasses has been modified in different ways.

Particularly, the inclusion of crystalline nanoparticles provides obstacles to SB propagation and growth, with SB often nucleating at the interface between the BMG and the nanoparticle. This results in a reduced and more homogeneous deformation in the plastic regime. Nevertheless, to ensure lasting effects, inclusions should be stable in time, i.e. not diffuse into the surrounding amorphous material loosing the sharp transition from crystal to amorphous.

In previous work we determined constitutive parameters of the $Cu_{46}Zr_{54}$ metallic glass as a function of temperature, using atomistic Molecular Dynamics (MD) simulations. We will now present results for spherical face-centered cubic (FCC) Cu inclusions. Although we do not focus on the size effects of inclusions like other studies, we analyze the stability of the nanoparticles at different temperatures. During mechanical deformation under uniaxial strain of a BMG sample with inclusions, we analyze Voronoi polyhedra, and shear stress and shear strain localization to study the role of the inclusion in the mechanical properties of this composite material.

1 INTRODUCTION

Bulk Metallic Glasses (BMG) are known for their outstanding mechanical properties such as elasticity, strength and hardness, and because of this they are matter of deep research. However, the tendency to massively collapse initially formed shear transformation zones (STZs) into a single shear band (SB) and thus failing catastrophically, restricts their plasticity and their applications [1, 2].

It is of much interest the modification of their composition so as to enhance these restraints [3, 4, 5]. In particular, the inclusion of crystalline nanoparticles promote the nucleation of STZs and act as an impediment to the propagation of SBs [3]. As a result, a reduced and more homogeneous deformation in the plastic regime is obtained.

After analyzing constitutive parameters of the $Cu_{46}Zr_{54}$ metallic glass used as matrix in this work [6], we now focus on the stability at different temperatures of spherical face-centered cubic (FCC) Cu inclusions using Molecular Dynamics (MD) simulations. Voronoi polyheadra, shear stress and shear strain are analyzed in the deformation process under uniaxial strain of the BMG in order to get a better understanding of the role of the inclusion in the mechanical properties of this composite material.

2 SIMULATION DETAILS

We use the LAMMPS software package [7] for running all the simulations, which is free and open source.

The original sample is a $Cu_{46}Zr_{54}$ metallic glass with 160k atoms, obtained with a quenching rate of 10^{12} K/s with an experimental glass transition temperature (T_g) of 696 K, and it has already been described in [8]. An embedded atom method (EAM) potential is adopted [9], used previously in other works on BMGs [1, 8, 10, 11, 12, 13]. Periodic boundary conditions are used in all directions, to mimic high strain rate loading conditions.

We analyze FCC Cu sphere-shaped inclusions. A spherical region of 2 nm radius was deleted from the sample in a central position which was then filled with the corresponding lattice, i.e. an FCC lattice with lattice constant of 0.3615 nm. After creating Cu atoms in the spherical region, the configuration was minimized, then equilibrated at zero pressure for few ps, then heated (or cooled) to reach the desired final temperature (T_f) during 4 ps and it was finally annealed at T_f for 1 ns.

The present work centers on the stability of these nanoparticles at different temperatures, although we show some cases of uniaxial tension and compression loading. Homogeneous strain rate of 10^9/s is applied. Diffusivity in all cases is computed fitting mean squared displacements (MSD), $\langle r^2 \rangle$, output from LAMMPS.

3 RESULTS

3.1 Inclusion Stability

In this section we analyze the stability of the nanoparticles at different temperatures, up to temperatures close to the glass transition.

MSD data for Cu atoms from the inclusion alone are obtained from simulations at different temperatures. As we can see in Figure 1 (a), after an initial transient behavior, the MSD becomes nearly constant, leading to a diffusivity close to zero, as expected for a stable solid inclusion.

This would indicate that the inclusions are indeed stable at normal operational conditions for BMGs. However, MD simulations are typically cover relatively short time spans of only few ns, and we move to higher temperatures for an improved assessment of nanoparticle stability.

We then use data for T $\geq$ 500 K (Figure 1 (b)), and obtain diffusivities shown in Table 1, using Einstein's equation $\langle r^2 \rangle = 6Dt$, for times longer than 0.6 ns, when there is a steady slope.

These results represent an average for all nanoparticle atoms, but there could be large differences between atoms in the core and the surface of the particle. Therefore, we calculate the MSD for Cu atoms within a spherical shell of thickness 0.8 nm, and inner radius of 1.2 nm. It can be seen in Figure 2 that, after a transient of around 0.6 ns, the slopes of the MSD are roughly the same for the shell and the entire nanoparticle, and we can use the diffusivities in Table 1.

Diffusivities for T $\geq$ 500 K are fitted to match equation 1, where k_B is the Boltzmann's constant and ΔE is the activation energy for diffusion, and D_0 sets the diffusivity scale. The resulting regression results appear in Table 2 and are displayed in Figure 3.

Table 1: Diffusivity fitting results

T $[K]$	D $[\frac{nm^2}{ps}]$	R^2
500	$8,490 \cdot 10^{-7}$	0,8306
600	$1,508 \cdot 10^{-6}$	0,9253
700	$4,699 \cdot 10^{-6}$	0,9357
800	$4,149 \cdot 10^{-5}$	0,9935

$$D = D_0 \cdot \mathrm{e}^{\frac{-\Delta E}{k_B T}} \tag{1}$$

As pointed out in [3], the crystalline core of inclusions shrinks because the external atoms tend to became amorphous. This effect increases with temperatures, as expected, when atomic diffusion is larger.

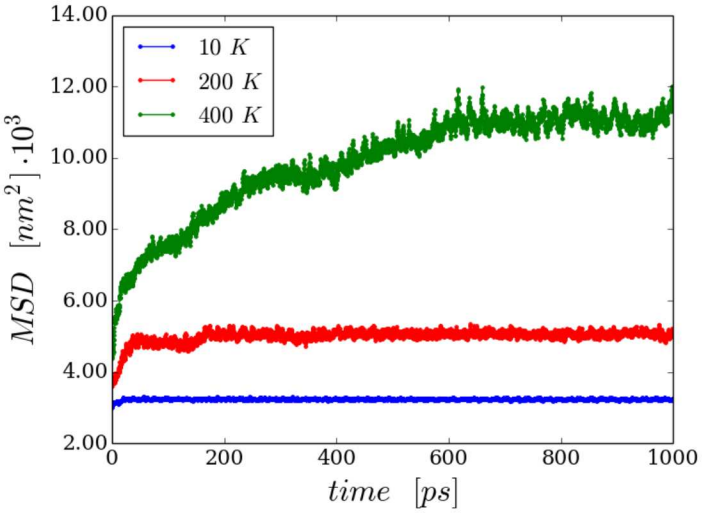

(a) Lower temperatures

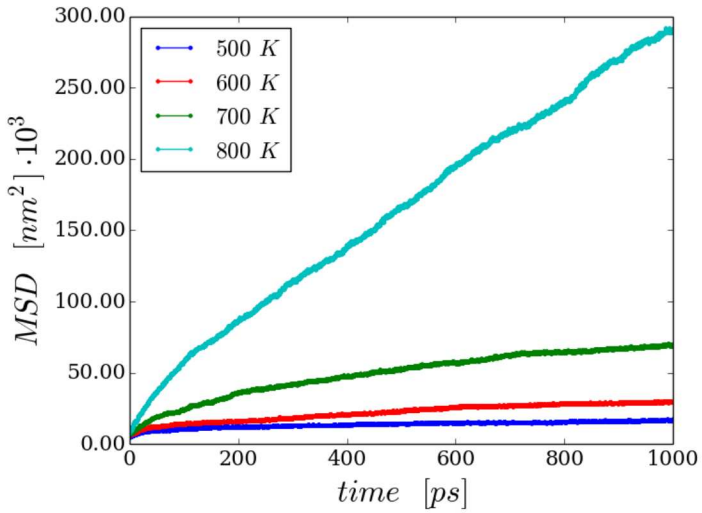

(b) Higher temperatures

Figure 1: MSD for FCC Cu inclusion at different temperatures

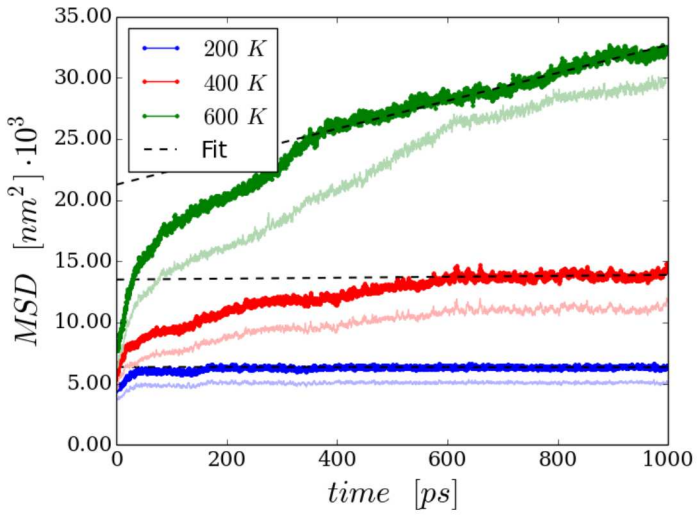

Figure 2: MSD of spherical shell and original for the whole sphere (lighter color)

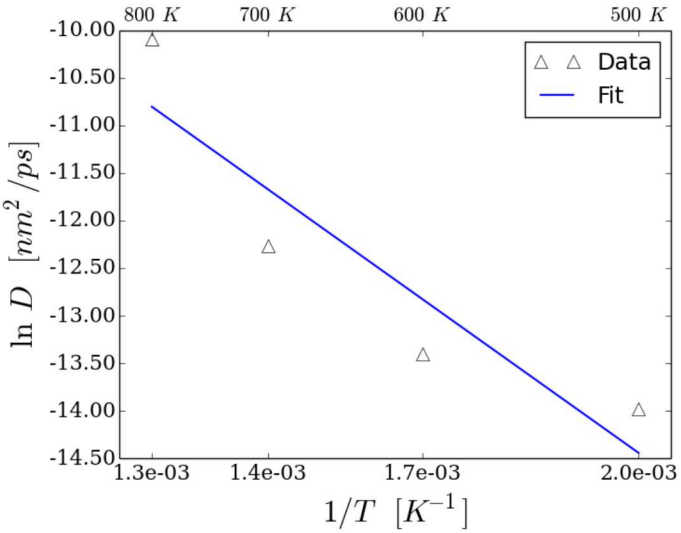

Figure 3: Diffusivity in function of temperature

Table 2: Diffusivity with respect to T fitting results

Activation energy $[eV]$	$-0,4182$
D_0 $[\frac{nm^2}{ps}]$	$8,771 \times 10^{-3}$
R^2	0,8399

3.2 Uniaxial Loading

In this section, we present results on uniaxial loading of the BMG containing a nanoparticle, as described before.

Figures 4 and 5 show the sample under uniaxial stress (tension and compression) for T = 10 K and 400 K. We consider these two temperatures as representative of a low temperature regime and a high temperature regime, but for temperatures for which diffusivity is small and the nanoparticle is stable.

The shape of the loading curves follows the expected behavior observed for the material without an inclusion [6]. The small inclusion does not affect the elastic regime, and at high temperature, the softening of the BMG is not affected either, neither in tension nor in compression. The maximum shear is slightly decreased by the nanoparticle at low temperatures. The flow stress at large strains is not modified by the inclusion under compression. On the other hand, the nucleation of a void under tension, indicated by the sudden drop in the stress, is slightly delayed by the inclusion, allowing about 1% additional strain of the sample. This might be due to some relaxation and dissipation taking place in the boundary between the nanoparticle and the BMG, but further studies are needed to clarify this.

Under tension (Figure 4), even if atomic shear strain seems to be concentrating at the boundaries of the inclusion located at the central zone of the sample as shown in Figure 6, homogeneous plastic strain is present, with nucleation of many STZs, probably due to the high strain rate and high quenching rate of the sample, leading to void nucleation in a zone different from the boundary between the BMG and the nanoparticle. Under compression at low temperature, there are also STZs, as shown in Figure 7.

As some particular Voronoi polyhedra are considered to be more shear resistant structures, particularly icosahedra clusters [14], we show the evolution of icosahedral fractions for the sample and compare it with the original BMG with no inclusion at 10 K. We can see in Figure 8 that fractions follow the same behavior as in the sample without a nanoparticle. Under tension, void nucleation leads to fluctuations. It is worth noting that these fluctuations correspond to a higher strain like we already mentioned for the stress-strain curve.

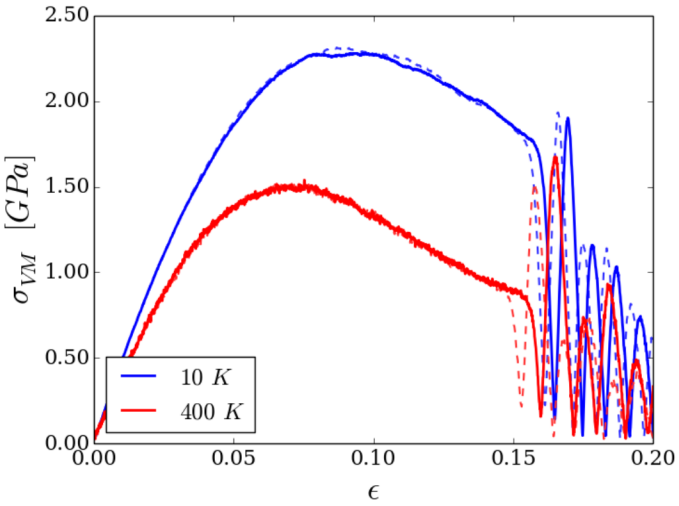

Figure 4: vonMises stress vs strain for the BMG under uniaxial tension with no inclusion (dotted line) and one inclusion (solid line)

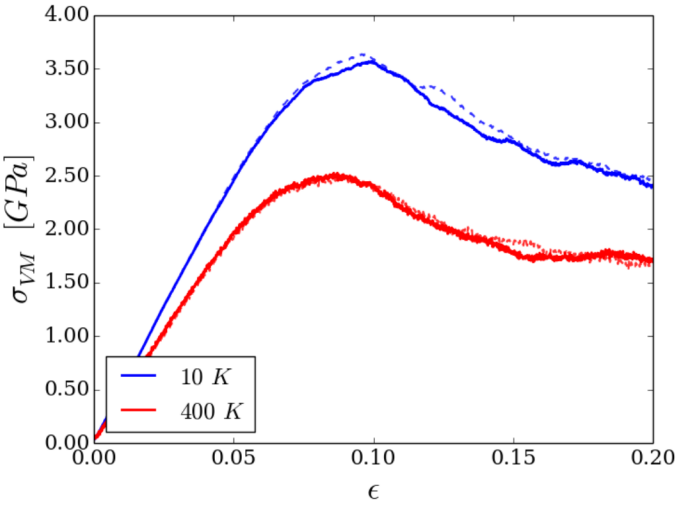

Figure 5: vonMises stress vs strain for the BMG under uniaxial compression with no inclusion (dotted line) and one inclusion (solid line)

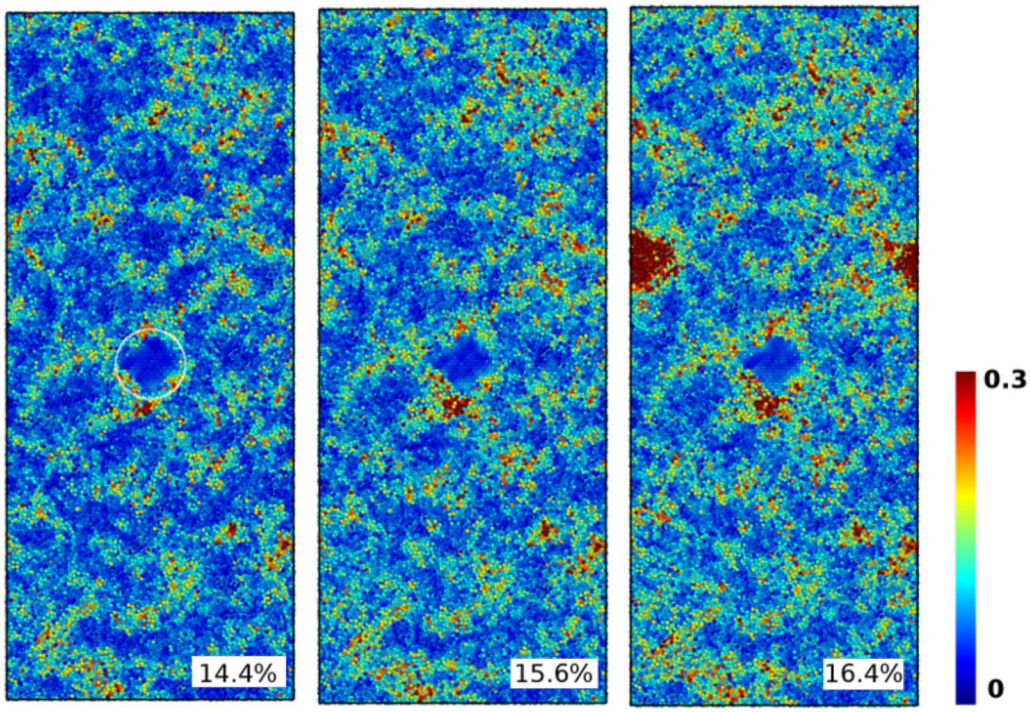

Figure 6: Snapshots of sample under tension at selected strains at 10 K (inclusion pointed out in first snapshot). Color represents atomic shear strain.

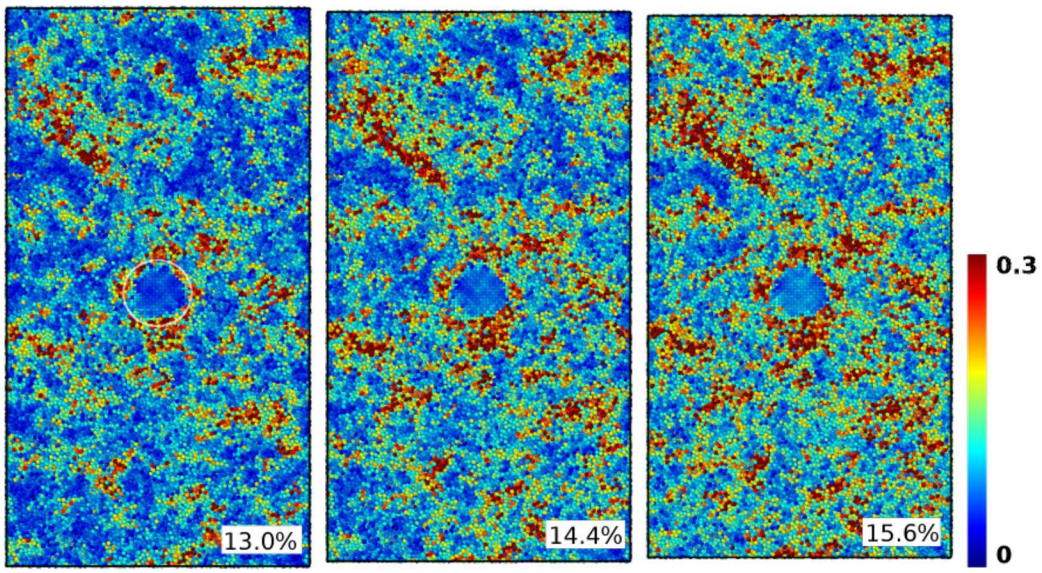

Figure 7: Snapshots of sample under compression at selected strains at 10 K (inclusion pointed out in first snapshot). Color represents atomic shear strain.

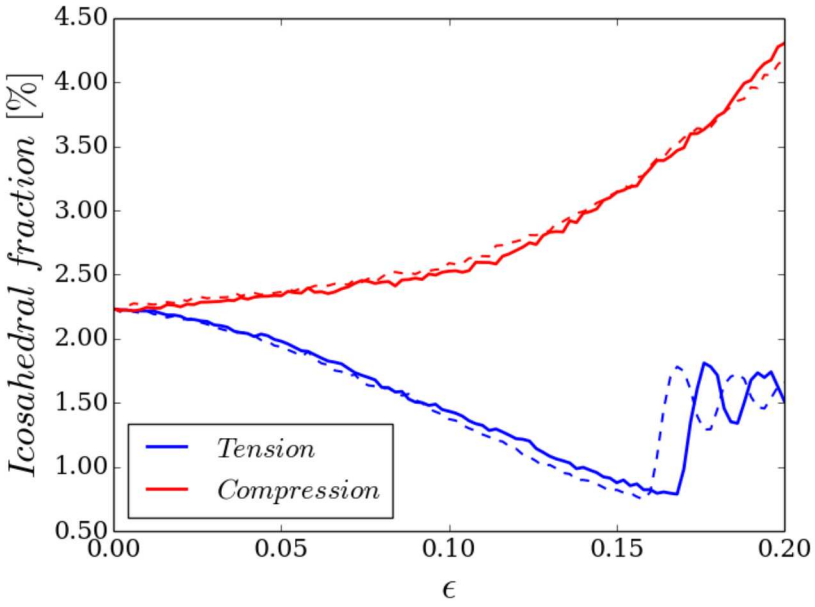

Figure 8: Icosahedral fraction under tension and compression at 10 K. Dotted line represents original sample.

4 SUMMARY AND CONCLUSIONS

We study a Bulk Metallic Glass with a crystalline nanoparticle as inclusion. We consider a CuZr glass, and a pure Cu nanoparticle with a radius of 2 nm. This implies a volume fraction that varies from 1.15% at 10 K to 1.12% at 800 K as a result of the increasing initial volume of the sample with temperature. A similar scenario was recently explored by Albe et al. [3]. Here we explore temperature effects, and initially we study the thermal stability below 400 K, indicating that the nanoparticle is fairly stable at those temperatures. At higher temperatures, diffusivity within few ns leads to the loss of a sharp interface between the nanoparticle and the glass.

In our simulations 3D-periodic boundary conditions where applied, and the absence of free surfaces leaves only the copper precipitate as likely stress concentrator to promote nucleation of STZs, as seeds for shear bands, at the interface between the nanoparticle and the glass. However, this was not the case. Stress-strain curves are fairly similar to the case without the nanoparticle, with the exception of a delay in void nucleation under tension for the sample with a nanoparticle.

Voronoi analysis did not show significant differences between the samples with and without the nanoparticle. Further voronoi analysis is required for different loading temperatures and loading conditions. Future studies will also repeat these experiments with

CuZr inclusions with a crystalline B2 structure, as found in some experiments [15, 16].

5 ACKNOWLEDGMENTS

We all thank support from SeCTyP-UNCuyo grant "B008 Study of possible improvements of the mechanical properties of metallic glasses". Eduardo M. Bringa also thanks support from PICT-PRH 0092.

REFERENCES

[1] A.J. Cao, Y.Q. Cheng, and E. Ma. Structural processes that initiate shear localization in metallic glass. *Acta Materialia*, 57:5146–5155, 2009.

[2] Q. Xiao, H.W. Sheng, and Y. Shi. Dominant shear band observed in an amorphous ZrCuAl nanowires under simulated compression. *MRS Communications*, 2:13–16, 2012.

[3] K. Albe et al. Enhancing the plasticity of metallic glasses: Shear band formation, nanocomposites and nanoglasses investigated by molecular dynamics simulations. *Mech. Mater.*, 67:94–103, 2013.

[4] S. Adibi et al. A transition from localized shear banding to homogeneous superplastic flow in nanoglass. *Appl. Phys. Lett.*, 103:211905, 2013.

[5] S. Adibi et al. Composition and grain size effects on the structural and mechanical properties of CuZr nanoglasses. *J. Appl. Phys.*, 116:043522, 2014.

[6] F. Ardiani et al. Atomistic simulations of amorphous metals in the elasto-plastic regime. *Mec. Comput.*, 31:1437–1449, 2012.

[7] S. Plimpton. Fast parallel algorithms for short-range molecular dynamics. *J Comp Phys*, 117:1–19, 1995. Site: http://lammps.sandia.gov.

[8] B. Arman, S.N. Luo, T.C. Germann, and T. Cağin. Dynamic response of $Cu_{46}Zr_{54}$ metallic glass to high-strain-rate shock loading: Plasticity, spall, and atomic-level structures. *Phys. Rev. B.*, 81, 2010. 144201.

[9] M. Daw and M.I. Baskes. Embedded-atom method: Derivation and application to impurities, surfaces, and other defects in metals. *Phys. Rev. B.*, 29:6443–6453, 1984.

[10] F. Shimizu, S. Ogata, and J. Li. Theory of shear banding in metallic glasses and molecular dynamics calculations. *Materials Transactions*, 48(11):2923–2927, 2007.

[11] Y.Q. Cheng, Ma E., and H.W. Sheng. Atomic level structure in multicomponent bulk metallic glass. *Phys. Rev. Letters*, 102, 2009. 245501.

[12] Y.Q. Cheng and E. Ma. Intrinsic shear strength of metallic glass. *Acta Materialia*, 59:1800–1807, 2011.

[13] C.C. Wang and g C.H. Won. Different icosahedra in metallic glasses: stability and response to shear transformation. *Scripta Materialia*, 66:610–613, 2012.

[14] Y. Q. Cheng et al. Relationship between structure, dynamics, and mechanical properties in metallic glass-forming alloys. *Phys. Rev. B.*, 78:014207, 2008.

[15] R. Wei, X.L. Wang, S. Yang, F. Jiang, and L. He. Formation of cuzr-based bulk metallic glass composites containing nanometer-scale b2-cuzr phase through sub-tg annealing. *J. Alloys Compd.*, 617(0):699 – 706, 2014.

[16] C.N. Kuo, J.C. Huang, J.B. Li, J.S.C. Jang, C.H. Lin, and T.G. Nieh. Effects of b2 precipitate size on transformation-induced plasticity of cu–zr–al glassy alloys. *J. Alloys Compd.*, 590(0):453 – 458, 2014.